Available online at www.sciencedirect.com
SCIENCE DIRECT®
International Journal of Solids and Structures 42 (2005) 2129–2144
INTERNATIONAL JOURNAL OF SOLIDS and STRUCTURES
www.elsevier.com/locate/ijsolstr

Numerical modelling of the structural behaviour of thin-walled cast magnesium components

C. Dørum [a,*], O.S. Hopperstad [a], O.-G. Lademo [b], M. Langseth [a]

[a] *Structural Impact Laboratory (SIMLab), Department of Structural Engineering, Norwegian University of Science and Technology, Richard Birkelands vei, 7491 Trondheim, Norway*
[b] *SINTEF Materials and Chemistry, 7465 Trondheim, Norway*

Received 23 October 2003; received in revised form 23 August 2004
Available online 13 October 2004

Abstract

Axial crushing, 3-point bending and 4-point bending tests have been performed in order to establish an experimental database of the behaviour of generic high pressure die cast (HPDC) AM60 structural components. In this paper, the experimental data are applied to obtain a validated methodology for finite element modelling of thin-walled cast components subjected to quasi-static loading. The HPDC structural components are modelled in LS-DYNA using shell elements. The cast magnesium alloy is modelled using both the classical J2-flow theory and an elastic–plastic model based on a non-associated J2-flow theory. In the latter, the constitutive model includes the Cockcroft–Latham fracture criterion, which is coupled with an element erosion algorithm available in LS-DYNA. It is further possible to define the fracture criterion as a Gauss-distributed stochastic parameter to allow for heterogeneities in the cast material. The constitutive model and fracture criterion are calibrated with data from tension and compression tests. Comparison of experimental and predicted behaviour of HPDC components gives promising results. It is found that the strength difference between uniaxial compression and tension has little influence on the numerical simulations. The fracture criterion of Cockcroft and Latham seems to be an effective approach to predict failure in HPDC components.

1. Introduction

Growing concerns for economy, environment and functionality have led to increased use of light-metals in the load carrying structure and safety components of cars. With high pressure die casting (HPDC) of magnesium and aluminium alloys, components with very complex, thin-walled geometry, like instrument

* Corresponding author. Tel.: +47 73594683; fax: +47 73594701.
E-mail address: cato.dorum@bygg.ntnu.no (C. Dørum).

0020-7683/$ - see front matter © 2004 Elsevier Ltd. All rights reserved.
doi:10.1016/j.ijsolstr.2004.08.019

Nomenclature

W	critical "plastic work" in Cockcroft–Latham fracture criterion
σ_1	maximum principal stress
σ_e	von Mises stress
ε_e	equivalent plastic strain
κ	material reference hardening
$\boldsymbol{\sigma}$	Cauchy stress tensor
$\boldsymbol{\varepsilon}$	true strain tensor
$\mathbf{C}$	elastic moduli
$\mathbf{I}$	second order unit tensor
$\boldsymbol{I}$	fourth order unit tensor
λ, μ	the Lamé constants

panels, A and B pillars and front end structures, can be cast with a high production rate. The challenge with the method is to optimise the process parameters with respect to the part design and the solidification characteristics of the alloy in order to obtain a sound casting without casting defects. Unbalanced filling and lack of thermal control can cause porosity and surface defects due to turbulence and solidification shrinkage. These defects can give low ductility compared to for instance extruded materials.

Design and production of thin-walled cast structural components for the automotive industry are challenging tasks, involving development of alloys and manufacturing processes, structural design and crashworthiness analysis. In order to reduce the lead time to develop a new product it is necessary to use finite element (FE) analysis to ensure a structural design that exploits the material. Accurate description of the material behaviour is essential to obtain reliable results from such analyses. To minimise the weight of the structural component while maintaining the safety in a crash situation, the ductility of the material has to be utilised without risking un-controlled failure. Hence, a reliable failure criterion is also required,

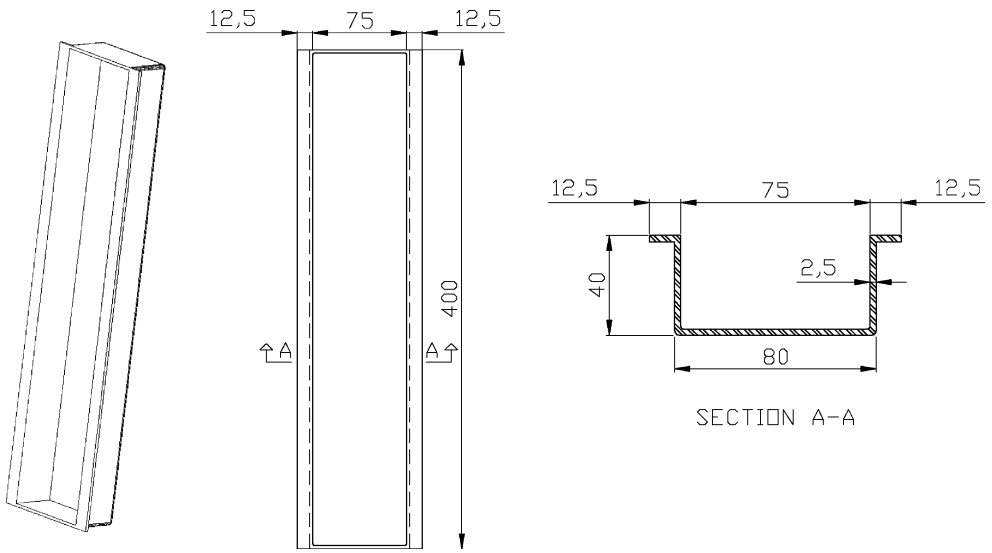

Fig. 1. Generic profile geometry without ribs.

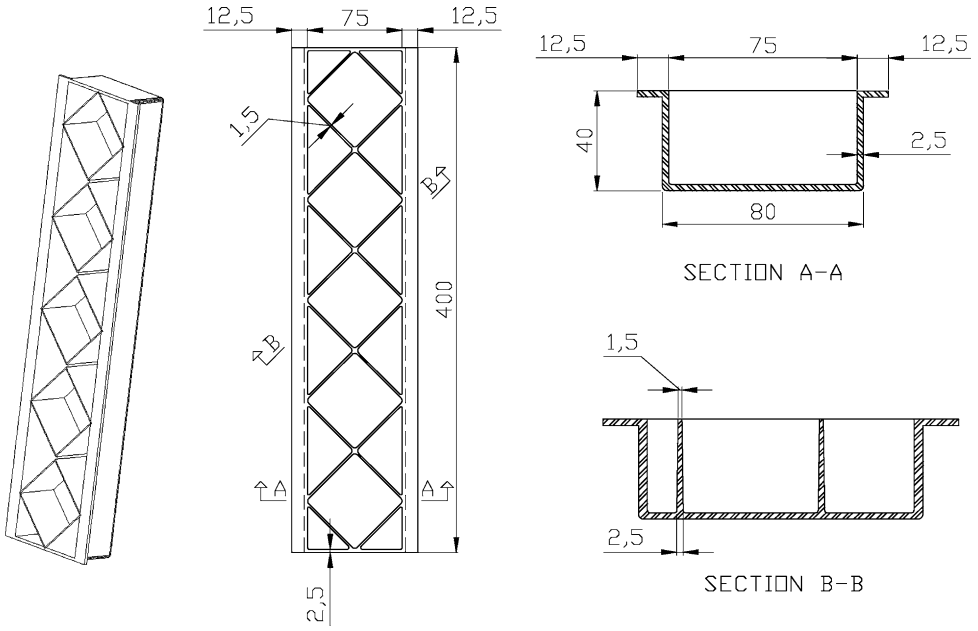

Fig. 2. Generic profile geometry with ribs.

giving limits for the plastic deformations under various loading combinations. Quite precise and validated constitutive models and failure criteria are available for materials such as extruded aluminium and rolled steel (Lademo, 1999). For thin-walled cast materials, however, much work is still to be done.

The long-term objective of this work is to develop design and modelling tools that allow the structural behaviour of thin-walled cast components to be predicted when subjected to static and dynamic loads. In the current study, the structural behaviour of generic structural HPDC components, shown in Figs. 1 and 2, has been investigated with the use of axial crushing, 3- and 4-point bending experiments. The components were cast of magnesium alloy AM60 at Hydro's Research Centre in Porsgrunn, Norway with a Bühler SC42D 420-ton cold chamber die casting machine.

2. Constitutive modelling

2.1. On the yield surface for cast AM60

Kelley and Hosford (1968) performed experiments showing that the yield surface of *textured* magnesium alloys takes complex shapes. Their conclusions were that the investigated polycrystalline materials were very anisotropic and that the anisotropy increased with increasing levels of texture. In addition, the yield surfaces were neither elliptical nor centred at the origin due to the directionality of the twinning mode, resulting in a different behaviour in tension and compression. Experimental results (Dørum et al., 2003) show that this strength difference also is present in the cast AM60 material, as shown in Fig. 3. Regarding the possibility for anisotropic material properties, modern and well controlled HPDC gives structural components with a very fine structure of randomly nucleated grains over the thickness. Based on these considerations it is probable that texture is negligible and, therefore, that the material is isotropic. Furthermore, experimental data (Laukli, 2002) shows that the material of the AM60 components indeed is isotropic.

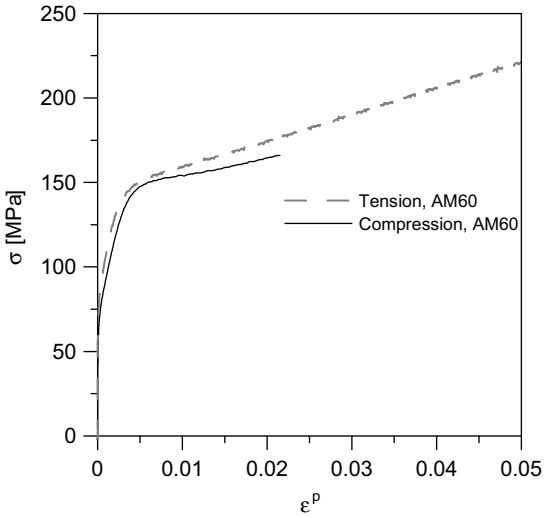

Fig. 3. Comparison of stress–strain curves obtained from uniaxial tension and compression tests for HPDC AM60.

Since the material is isotropic, it was chosen to simulate the bending and axial loading experiments of the generic components with the use of the classical J2-flow theory. The J2-flow theory is based on the von Mises yield surface with isotropic hardening and associated flow rule. However, for this approach to be valid, the difference in tension and compression properties for the HPDC AM60 is required to be negligible. The essential assumption of the J2-flow theory is that plastic flow in metals is unaffected by pressure, as demonstrated experimentally by Bridgman (1949). In the J2-flow theory, the yield condition and the associated plastic flow direction are based on the deviatoric part of the stress tensor. To investigate the effect of the reported strength difference, the experiments are also simulated using a pressure sensitive material model implemented in this work.

It has been shown by Rice (1971) that the normality condition is a direct consequence of the assumption of crystal slip obeying Schmid's law. However, Li and Richmond (1997) stated that examination of the physical bases of plastic deformation of materials indicates that metals and alloys, as well as geomaterials, exhibit non-normality to some extent from appreciable to negligible. That is, the incremental plastic strain vector is not necessarily normal to the current yield surface. Furthermore, if plastic deformation exhibits some sort of pressure sensitivity, while the plastic dilatancy or volume change associated with the plastic deformation is moderate or non-existent, non-normality (non-associated flow) results. Metals that exhibit different yield strengths under uniaxial compression than under uniaxial tension, known as the strength differential (SD, Drucker (1973)) effect, may, according to Li and Richmond (1997), be viewed as one manifestation of pressure effects on yielding. The non-associated extended J2-flow theory with pressure sensitive hardening, which is adopted in this work, is designed to model the behaviour of metals with strength differential (SD) effects. Therefore, the material model will in this work be referred to as the SD model. In the SD model, the von Mises yield surface is modified along the axis of normalised pressure such that different hardening properties can be given for two different user-defined values of normalised pressure. Similar to the yield condition for the non-associative J2-flow theory discussed by Simo and Taylor (1985), the yield surface for the SD model can be expressed as:

$$f(\boldsymbol{\sigma}, \varepsilon_e) = \sigma_e - \kappa(\mathrm{tr}\,\boldsymbol{\sigma}/\sigma_e, \varepsilon_e) = 0 \tag{1}$$

where σ_e is the effective von Mises stress, and ε_e is the corresponding effective plastic strain. The term $\mathrm{tr}\,\boldsymbol{\sigma}/\sigma_e$ represents a normalised pressure or a triaxiality parameter. κ represents the current yield stress, or the

Table 1
SD model (a non-associated J2-flow theory)

Strain rate decomposition:	$d\boldsymbol{\varepsilon} = d\boldsymbol{\varepsilon}^{e} + d\boldsymbol{\varepsilon}^{p}$
Incremental stress–elastic strain relation:	$d\boldsymbol{\sigma} = \mathbf{C}{:}d\boldsymbol{\varepsilon}^{e} = \mathbf{C}{:}(d\boldsymbol{\varepsilon} - d\boldsymbol{\varepsilon}^{p})$ where $\mathbf{C} = \lambda \mathbf{I} \otimes \mathbf{I} + 2\mu \boldsymbol{I}$
Incremental plastic strain vector:	$d\boldsymbol{\varepsilon}^{p} = d\lambda \frac{\partial \sigma_e}{\partial \boldsymbol{\sigma}}$ where $\sigma_e = \sqrt{\frac{3}{2}\boldsymbol{\sigma}^{dev} : \boldsymbol{\sigma}^{dev}}$
Yield criterion:	$f = \sigma_e - \kappa(\mathrm{tr}\,\boldsymbol{\sigma}/\sigma_e, \varepsilon_e) \leqslant 0$ where $d\varepsilon_e = \frac{1}{\sigma_e}\boldsymbol{\sigma} : d\boldsymbol{\varepsilon}^{p}$
Loading/unloading conditions:	$f \leqslant 0,\ d\lambda \geqslant 0,\ f \cdot d\lambda = 0$

hardening properties, and is given as a function of both the effective plastic strain and the normalised pressure. The flow potential, defining the direction of the incremental plastic strain vector, is given by the von Mises effective stress. A more detailed description of the SD model is given in Table 1. The model is formulated for small deformations. In the implementation, large plastic strains and large rotations are accounted for using a co-rotational formulation for shell elements and a hypoelastic–plastic formulation for brick elements based on the Jaumann stress rate (see e.g. Belytschko et al., 2000).

At two points of user-defined normalised pressure, pn_1 and pn_2 ($pn_1 > pn_2$), the model is calibrated with material tests. If the normalised pressure is greater than or equal to pn_1, then the hardening is equal to the hardening curve given as a user-defined curve at pn_1. Furthermore, if the normalised pressure is less than or equal to pn_2, then the hardening follows the hardening curve given as a user-defined curve at pn_2. Between the points of user-defined normalised pressure, as illustrated in Fig. 4, a linear interpolation is used. In this work, the yield properties are prescribed at the points of uniaxial tension and uniaxial compression as illustrated in Fig. 4. This enables the model to be calibrated with relatively simple experiments. Here, the SD model is calibrated with the uniaxial compression and uniaxial tension experiments performed by Dørum et al. (2003) and Laukli (2002).

The data from the compression test cover only a range in effective plastic strain from 0% to 2%, while the data from the tensile test cover a range from 0% to 9%. To be used in the numerical simulations, the experimental data from the compression test must be extrapolated to cover a wider range in effective plastic strain. For *textured* pure magnesium, Kelley and Hosford (1968) have shown that the difference in uniaxial

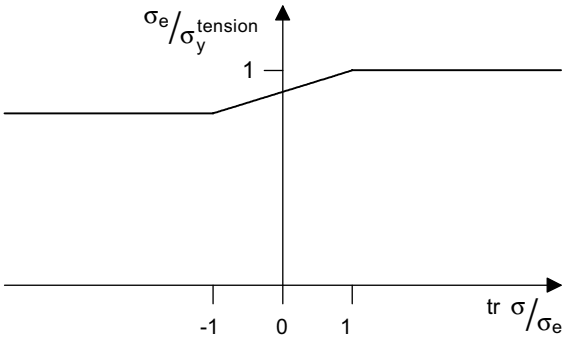

Fig. 4. Yield surface for the SD model.

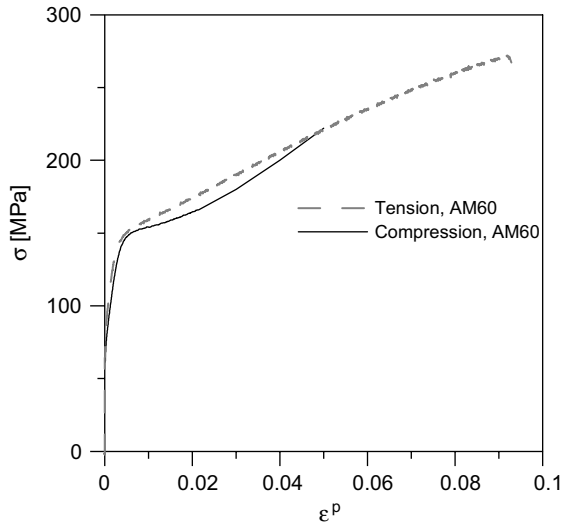

Fig. 5. Reference hardening curves for uniaxial tension and compression.

tensile and compressive properties is significantly reduced at 10% plastic strain. Here, working with the high pressure die cast AM60 material with randomly distributed grains, it has been chosen to eliminate the SD effect at an effective plastic strain of approximately 5%. For larger strains, the reference hardening curve in uniaxial compression is chosen to follow the reference hardening curve in uniaxial tension. Between 2% and 5% plastic strain, stress–strain points are chosen to give a smooth stress–strain curve. The reference hardening curves are shown in Fig. 5. By choosing equal reference hardening curves for uniaxial tension and compression, the SD model will be reduced to the classical J2-flow theory.

2.2. Fracture criterion

In the SD model, a criterion of ductile fracture proposed by Cockcroft and Latham (1968) is added. The fracture criterion is coupled with the element-kill algorithm available in LS-DYNA. As the fracture criterion is reached in one layer of an element, this element is removed (eroded) from the finite element model. In describing material failure, element removal is not the physically correct approach. However, in this work, the crack propagation itself is not considered to be as important as the onset of failure. The Cockcroft–Latham criterion can be expressed as:

$$W = \int \max(\sigma_1, 0)\, \mathrm{d}\varepsilon_e \leqslant W_c \tag{2}$$

where σ_1 is the maximum principal stress. This criterion implies that fracture is a function of the tensile stresses and equivalent plastic strain and has the dimensions of work per unit volume. If the maximum principal stress is compressive, fracture cannot occur. Furthermore, neither stresses nor strains alone are sufficient to cause fracture.

The critical value of ''plastic work'', W_c, can then easily be calibrated against uniaxial tension tests. In the SD model, the value of W_c can also be given as a stochastic parameter for each integration point, by introducing a Gauss distribution where a value for W_c is calculated in the first time step. With this approach, the structural behaviour of the generic HPDC components can be studied with statistical effects taken into account. This is a first attempt to represent effects of the inhomogeneous properties resulting from the casting process.

2.3. Numerical implementation

The SD model is implemented in LS-DYNA (Theoretical Manual, 1998) for co-rotational shell elements in plane stress, i.e. the out-of-plane normal stress is assumed to be zero. In the implementation, the out-of-plane shear stresses are treated elastically; i.e. only the in-plane stress components enter into the constitutive model of elastoplasticity. For the shell elements, the stress update is based on the fully-implicit backward Euler method (Belytschko et al., 2000). The SD model is also implemented for brick elements, but then using the radial return method proposed by Simo and Taylor (1985).

3. Component tests and numerical simulations

Numerical simulations of the generic structural high pressure die cast components are performed using LS-DYNA. The components are modelled using shell elements, and both the classical J2-flow theory and the SD model are considered. Axial loading, 3-point and 4-point bending are simulated, and the numerical results are then compared with experimental force–deformation characteristics. A schematic illustration of the studied load cases is provided in Fig. 6. The investigated components are of the magnesium alloy AM60, with an initial strength difference in uniaxial compression compared to uniaxial tension of approximately 10%.

In the 3- and 4-point bending tests, the load was applied on both the wide flange as shown in Fig. 7 and on the small flanges as shown in Fig. 8. The first load case will be referred to as (n), and the second load case will be referred to as (u). The components were tested in an Instron 1126 machine under displacement control, with a rate of displacement of approximately 20 mm/min. Measurement of the applied load and the corresponding displacement was carried out using Instron Labtronic 8800. More details concerning the 3- and 4-point tests are given by Dørum et al. (2003) and Sannes et al. (2003).

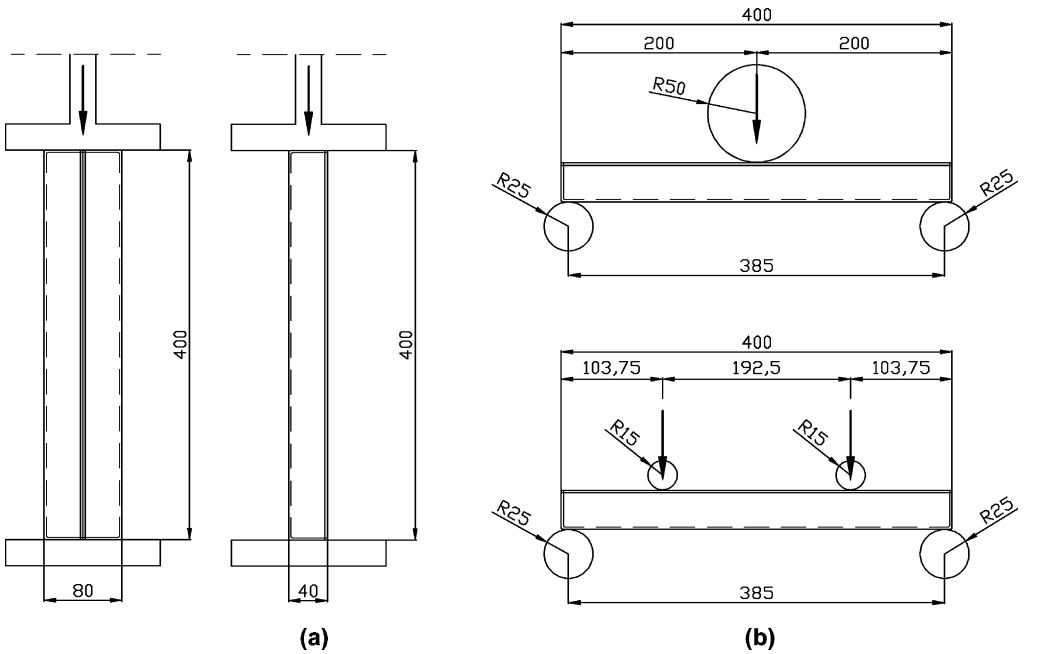

Fig. 6. Schematic illustration of (a) axial loading and (b) 3- and 4-point bending.

Fig. 7. Test set-up for 3-point bending, load case (n).

Fig. 8. Test set-up for 3-point bending, load case (u).

In axial loading, the load was applied through a rigid plate of high strength steel. Both single and double components with and without reinforcing ribs were tested, as shown in Fig. 9. The double profiles were manufactured by joining two single profiles with screws along the small outer stiffeners. The components were placed on a horizontal steel plate, and tested in an Instron 1126 machine under displacement control, with a rate of displacement of approximately 50 mm/min. As for the bending experiments, the measurement of load and displacement was carried out using Instron Labtronic 8800. A more detailed description of the axial loading tests is given by Dørum et al. (2003).

The material models are calibrated based on stress–strain curves obtained from uniaxial tensile and compression tests with specimens machined from the mid-section of the wide flange of the AM60 components without ribs. Consequently, the porosity and void growth in the cast material is directly taken into account in the plastic domain. For simplicity, the elastic properties are assumed to be unaffected by the porosity. It should be noted that this simple approach assumes that the porosity is uniformly distributed throughout the component. No information on local porosity levels in the casting is available, and it cannot be concluded that the porosity in the tensile specimens reflects the overall porosity. However, experimental work by Sannes et al. (2003) shows that the variations in yield stress are very small between different areas of the casting. The failure criterion adopted in the SD model is calibrated with the same uniaxial tensile tests that gave the reference hardening curves described above. With this procedure, the critical value of W_c as defined in (2) was found to be equal to 12.9 MPa. Details concerning the material tests are given by Dørum et al. (2003).

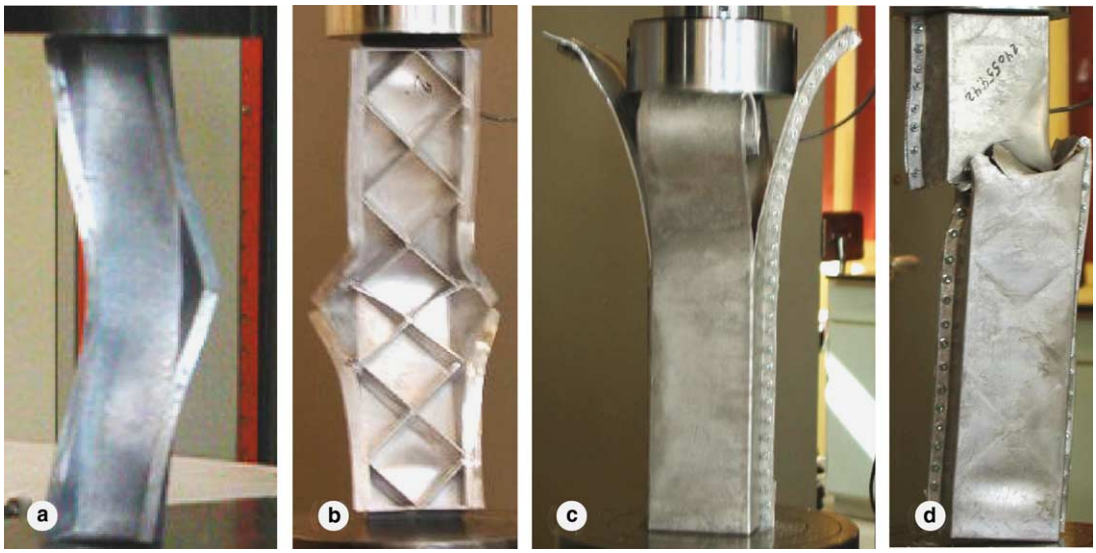

Fig. 9. Axially crushed profiles (a) single profile without ribs, (b) single profile with ribs, (c) double profile without ribs and (d) double profile with ribs.

Numerical simulations were carried out using the explicit FE-code LS-DYNA. The FE-models of the components without and with ribs are shown in Fig. 10, and they consist, respectively, of 5000 and 7000

Fig. 10. FE models of the generic components.

Belytschko–Tsay shell elements with one point integration in the plane and five through the thickness. The relatively fine mesh was chosen to give a good description of buckling as well as being able to include a reasonable description of the material inhomogeneities. Simulations with a finer mesh were also carried out to investigate the mesh-sensitivity. It was found that increasing the mesh density with a factor 1.5 did not have any significant influence on the results from the numerical simulations. Therefore, it was concluded that the chosen number of elements was appropriate. Double components were modelled by joining two single components with the contact type contact tied shell edge to surface constrained offset. With this approach, contact is established between the single components along the whole area of their small outer flanges, while in the experiments the components are joined with screws. However, the screws are relatively close-spaced and the chosen numerical approach is therefore assumed to correctly represent the structural behaviour of the outer flanges. The FE-models of the double components without and with ribs then consist of 10,000 and 14,000 shell elements, respectively.

In the simulations of the bending and the axial crushing tests, the deformation was applied through rigid body motion of cylinders and plates, respectively, in which the material was assumed rigid. The deforma-

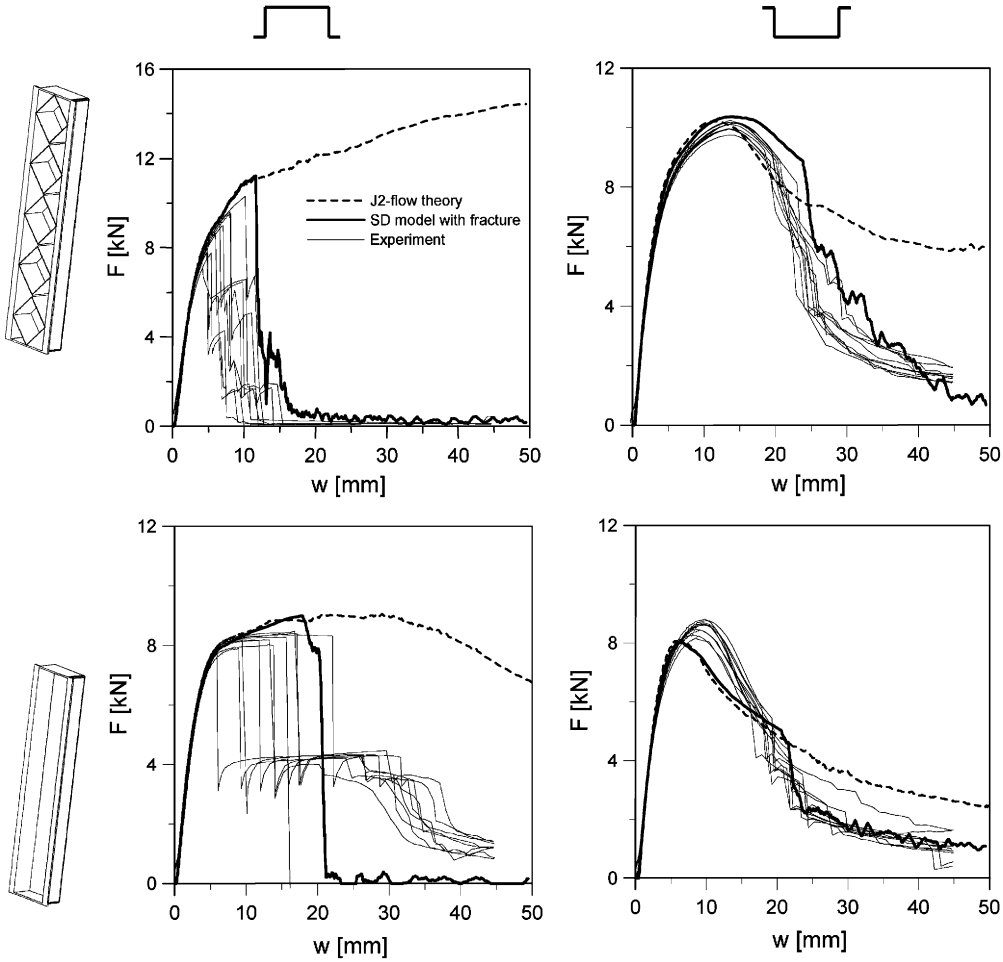

Fig. 11. Comparison of force–deformation characteristics of AM60 components subjected to 3-point bending.

tion was applied *smoothly* but much faster than in the experiments. However, the analysis can be regarded as quasi-static, and therefore comparable with the experimental results, provided the kinetic energy and its variation are both negligible throughout the simulation. This was checked for all simulations.

The comparisons of force–deformation characteristics obtained from the numerical analyses and the experiments are shown in Figs. 11 and 12 for 3-point and 4-point bending, respectively. For the simulations using the SD model with the Cockcroft–Latham fracture criterion, the data has been smoothened using a 9-point running average (total number of data points for each of the simulations is 1000) to give a better visualisation of the force–deformation characteristics after fracture has occurred. It is seen from the experimental results that the components subjected to bending in the n-mode show a relatively large scatter in structural ductility. This is because the structural capacity of the components here is limited by tensile failure of the small flanges. When loaded in the n-mode, the small flanges experience approximately uniaxial tension. The inhomogeneous micro-mechanical structure present in the HPDC AM60 components causes large differences in local tensile ductility. Consequently, as a large scatter was found in tensile elongation from uniaxial tensile tests (Laukli, 2002; Sannes et al., 2003), the scatter in structural response must be expected to be of the same order. Most significant is the scatter for the case of 3-point bending in the n-mode, where fracture always occurs at the small outer flanges at or close to the midpoint of component.

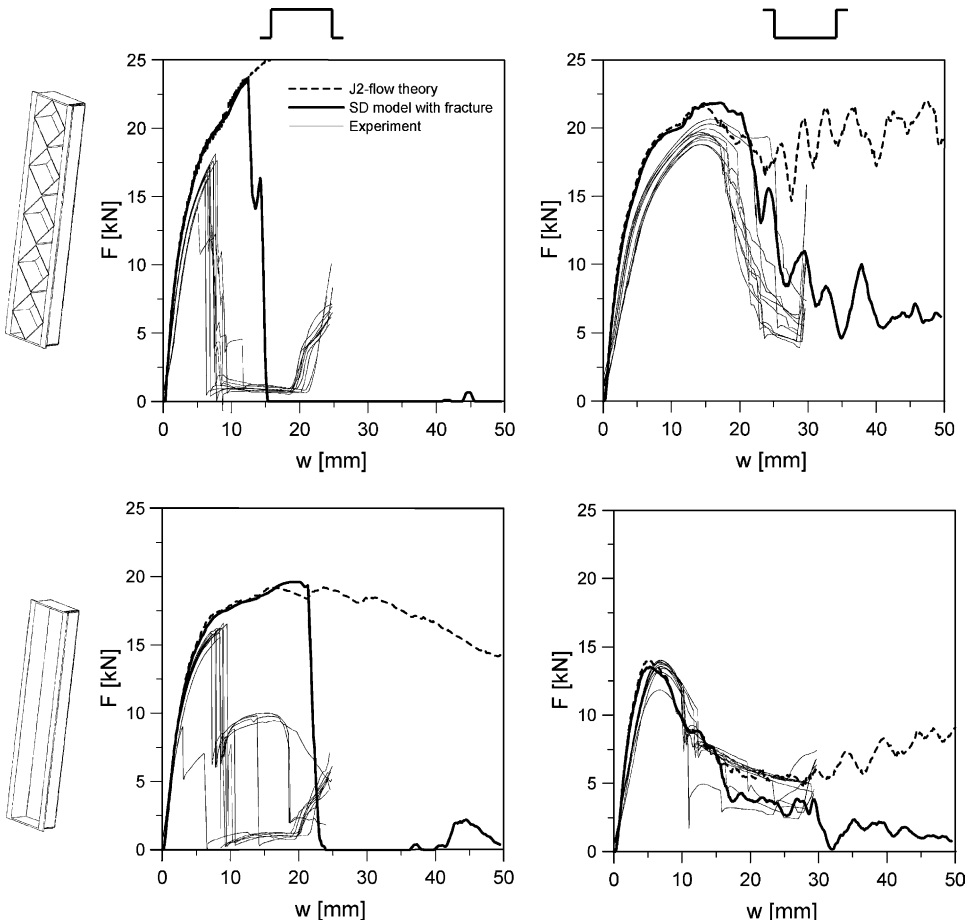

Fig. 12. Comparison of force–deformation characteristics of AM60 components subjected to 4-point bending.

For the case of 4-point bending, larger sections of the small flanges experience the same tensile loading. Owing to statistical effects, the probability for the critical section of the flanges to have a low tensile ductility is therefore larger for the case of 4-point bending than for 3-point bending. Thus, the reduced scatter in 4-point bending (n-mode) compared to the scatter in 3-point bending is reasonable. Generally, for the bending experiments in n-mode, the components with ribs show a less ductile behaviour than the ones without ribs.

For the components loaded in the u-mode, a very small scatter in force–deformation characteristics is found. Here, the first part of the force–deformation characteristics, i.e. before any fracture takes place, is limited by local buckling of the side webs and the compression flanges. The buckling phenomenon is controlled by the material hardening, slenderness and initial imperfections of the profile. After the buckling load has been reached, the plastic deformation in the buckles increases rapidly as the buckles develop further and fracture occurs. Thus, relative to the global force–deformation behaviour, the variations in local tensile ductility are of little importance, and the small scatter should be expected.

The figures further show that the structural response of the components subjected to bending is captured very well in the numerical simulations. Furthermore, it is seen that the failure criterion adopted in the SD model predicts failure quite accurately for the bending experiments in u-mode. As an example, the simulation of AM60 component with ribs subjected to 3-point bending in the u-mode (Fig. 11), show that maximum load is reached after a global deformation w of approximately 14 mm. Then, material failure is predicted when $w = 24$ mm. This gives a softening effect compared to the simulation using the J2-flow theory where failure is not included. For the n-mode, it is seen that the simulations using the SD model predict a structural response that is somewhat too ductile. Here, fracture occurs at the small flanges that experience approximately uniaxial tension. Experimental work performed by Sannes et al. (2003) show that the tensile ductility varies significantly throughout the cast component. The poorest area is the small flanges where elongations as low as 2–3% have been measured. The wide flange, from where the specimens for calibration of the failure criterion were taken, showed much better properties with elongation in the range of 12–16%. Thus, in the bending experiments in n-mode, the largest strains in the components are found where the mechanical properties are poorest. Therefore, the difference between the simulations and the experiments with respect to structural ductility is expected. To improve the predictions of material failure, it is vital that W_c is given a realistic distribution throughout the component. Rather than improving the predictions by dividing the component into different material parts with different W_c values, the idea here is to start with constant material properties, and, at a later stage, create a distribution using defect predictions from a casting simulation.

For the case of axial loading, the comparison of experimental force–deformation characteristics with results from numerical simulations is shown in Fig. 13. Here, the obtained experimental results have the same properties as the bending experiments in u-mode with respect to scatter in force–deformation behaviour. The deformation is mainly controlled by buckling and the variations in local tensile ductility do not have any important effect on the overall structural response. As for the bending experiments in u-mode, the predicted structural behaviour from the numerical simulations fits well with the experiments, especially for the components without ribs. The simulations of the components with reinforcing ribs predict a higher sustainable load than found from the experiments. As the material models were calibrated using specimens machined from components without reinforcing ribs, it is uncertain whether the obtained reference hardening curves represent the mechanical properties in the components with ribs. Thus, this difference in load level can be caused by inaccurate description of the mechanical properties as well as inaccurate description of the geometrical inhomogeneity. However, the fracture criterion proposed by Cockcroft and Latham seems to describe the structural ductility very well. More details concerning the experimental work is given by Dørum et al. (2003) and Sannes et al. (2003).

Numerical prediction of the local buckling phenomenon is known to be dependent upon a reasonable description of the initial geometrical imperfections. These were not measured for the tested generic components, but modelled using superposition of sine waves in the length and width directions. In previous work

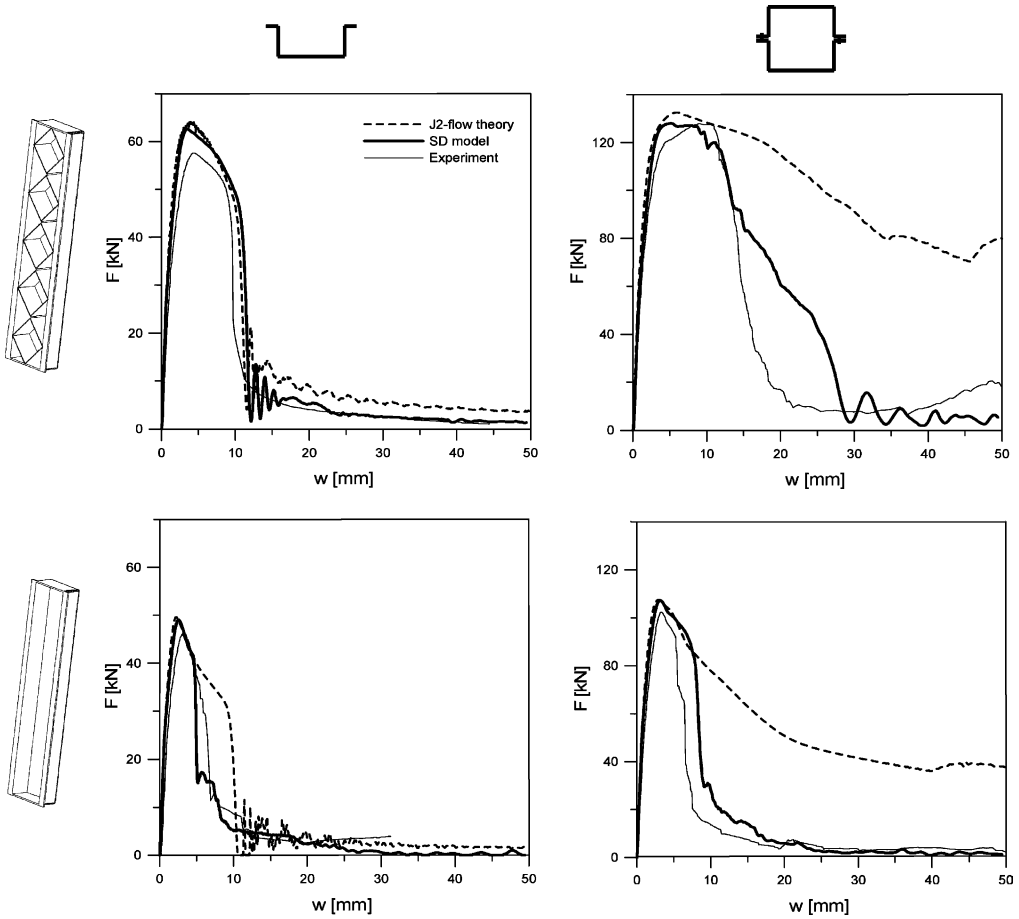

Fig. 13. Comparison of force–deformation characteristics of AM60 components subjected to axial crushing.

by the authors (Dørum et al., 2003), a sensitivity study was performed with respect to the geometrical imperfections. Based on the results from this sensitivity study, it was chosen to use a local sine-wave imperfection with amplitude of 0.5 mm, and a global sine wave with amplitude of 2.0 mm. It should be noted that visual inspection of the cast components confirms that the chosen geometric imperfection amplitudes are of a reasonable magnitude. As Figs. 11–13 demonstrate, the force–deformation characteristics obtained from the numerical simulations fit reasonably well with the experimental behaviour before fracture takes place. Thus, both the J2-flow theory and the SD model capture the structural behaviour of HPDC AM60 components. It can be concluded that the difference between the tensile and compressive uniaxial stress–strain curves as shown in Figs. 3 and 5 have no significant influence on the numerical predictions in these cases. The largest differences in force level between the simulations and the experiments are found for the single components with ribs subjected to axial loading. This may be caused by a poor description of the material and geometrical inhomogeneities for these components. There have not been performed any investigations regarding the material quality for the components with ribs. However, large surface defects can easily be found by visual inspection of the ribs. The true strength of the components with reinforcing ribs is therefore probably too high in the simulations since the material models are calibrated with specimens from the wide flange of components without ribs where the material quality probably is significantly better.

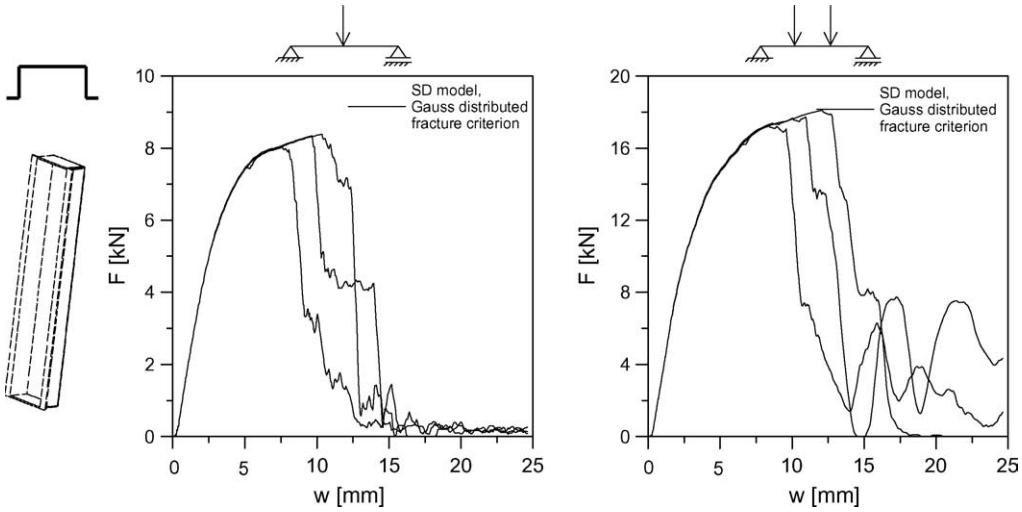

Fig. 14. Numerical simulations of 3- and 4-point bending, with the fracture criterion introduced as a Gauss-distributed stochastic variable.

From the simulations of the bending experiments in the n-mode, it was found that the adopted fracture criterion predicted too ductile structural response compared to the experiments. The reason for this was explained with the reported variations in tensile elongation (Laukli, 2002; Sannes et al., 2003). To investigate the effect of variations in local tensile ductility, W_c was defined as a Gauss distributed stochastic parameter, and the cases of 3- and 4-point bending in the n-mode for the components without ribs were reanalysed. Six simulations with identical input parameters were run for each load case. The material properties are assumed to be statistically independent between the integration points. The typical force–deformation characteristics from these analyses are shown in Fig. 14. From tensile tests (Laukli, 2002) using specimens from different locations of the AM60 component, a set of 22 different values for the fracture parameter W_c was calculated. Assuming that the experimental values of W_c were following a Gauss distribution, the mean value of the distribution was estimated to be 15.6 MPa, and the standard deviation was estimated to be 4.0 MPa. In the simulations, the value of W_c for each integration point was calculated at the first time step using a random number generator. Thus, two different simulations with equal input files will then generate different distributions of W_c, and also give different predictions of the structural ductility. As shown in Fig. 14, this approach gives a prediction of fracture at displacements in the range of 8–11 mm for 3-point bending, and 8–12 mm for 4-point bending. The corresponding range observed in the experiments is 6–22 mm and 7–10 mm for 3-point bending and 4-point bending, respectively. Compared to the force–deformation characteristics shown in Figs. 11 and 12, this approach gives better agreement with the experimental results, than found with the simulations using a constant value of W_c equal to 12.9 MPa. However, while the scatter in structural ductility observed in the experiments is similar to what is observed in the simulations of 4-point bending, this is not the case for 3-point bending. With a more realistic distribution of W_c, even better results could probably be achieved.

4. Concluding remarks

The long-term objective of this work is to develop design and modelling tools that allow the structural behaviour of thin-walled cast components to be predicted when subjected to static and dynamic loads such

as in crash situations. The approach consists of the following ingredients: casting of generic components relevant for the automotive industry, material and component testing, constitutive modelling and validation simulations using the finite element method.

In the present study, high pressure die cast AM60 components were subjected to axial crushing and 3- and 4-point bending. Laboratory experiments and explicit finite element simulations with shell elements were performed. Only quasi-static loading conditions were considered. An elastic–plastic constitutive model based on a non-associated extended J2-flow theory, referred to as the SD model, was implemented in the FE-code LS-DYNA. The SD model is designed to model the behaviour of metals with strength differential (SD) effects, and is calibrated against uniaxial tension and uniaxial compression tests. The fracture criterion proposed by Cockcroft and Latham (1968) was adopted for the SD model, and can be defined as a Gauss-distributed stochastic parameter. This option makes it possible to introduce material inhomogeneities in the cast material and reproduce the stochastic nature of the casting process. That is, components cast with equal process parameters can get a different distribution of the material properties.

In general, experimental results presented both in this work and by Dørum et al. (2003) show that there exists a relatively large scatter in the force–deformation behaviour when the HPDC components are subjected to deformation modes where the failure depends on the local tensile ductility of the material. For deformation modes where the force–deformation behaviour is controlled by local buckling much less scatter is found.

From numerical simulations with LS-DYNA, it was found that both the classical J2-flow theory and the SD model capture the structural behaviour of the generic AM60 components with reasonable accuracy. Thus, for the load cases studied here, it can be concluded that the reported strength differential effect in the cast AM60 material found from uniaxial tension and compression tests have no significant influence on the accuracy of the numerical simulations in terms of force–deformation behaviour. This observation is related to the fact that the measured force–deformation characteristics can be viewed as an integrated response, where the applied force at a given displacement is a function of the stress and strain distribution in the component. Consequently, whether the difference in compressive and tensile yield stresses influence the global response depends upon the load case and the geometry of the component. Even if the J2-flow theory captures the force–deformation behaviour for these cases, it does not have the ability to reproduce the uniaxial properties of the AM60 material. Further, existing experimental data for other die cast magnesium alloys, such as the AE42 alloy, show that the SD effect can be significantly larger (tensile yield strength equal to 145 MPa and compressive yield strength equal to 103 MPa) (Hydro Magnesium, 1998). Largest deviation from the experimental force–deformation characteristics was found in the simulations of single components with ribs subjected to axial loading. This deviation may be due to inaccurate description of both the geometrical and material inhomogeneities. No experimental data are available concerning the material quality of the components with reinforcing ribs. However, several surface defects can be found by visual inspection.

The fracture criterion proposed by Cockcroft and Latham (1968) gave promising results. Especially the structural ductility of components subject to axial crushing and bending in the u-mode was quite accurately predicted using a constant value of W_c. The reason for the good agreement in these cases is related to the evolution of local plastic strains with increasing global deformation after the buckling load has been reached. Here, a small increase in global deformation results in a relatively large increase in local plastic strains. Thus, the accuracy of the prediction of failure in terms of global force–deformation behaviour is not very dependent on the accuracy of the W_c parameter. For the case of bending in n-mode, the simulations using a constant value of W_c predicted too ductile response. To represent the scatter found in the experimental force–deformation behaviour and the scatter in local tensile ductility, two series of simulations were run with the critical plastic work in the fracture criterion introduced as a stochastic Gauss-distributed variable. The Gauss distribution was generated from experimental results provided by Laukli (2002). With this approach, a better agreement with the experiments was observed. In this work, the

fracture criterion is only used in combination with the SD model. However, for the load cases studied here, the fracture criterion would probably give equally good agreement with the experiments also if it had been implemented in the J2-flow plasticity model. For the load cases axial crushing and bending in the u-mode, the simulations where fracture criterion is not included make it possible to see how the material failure affects the softening branch of the force–deformation characteristics after the buckling load has been reached.

In order to further improve the simulations with respect to the description of structural ductility, a more realistic distribution of the inhomogeneity present in the components should be included in the FE-models. Thus, a coupling between a die casting process simulation and the pre-processor for the final FE-simulations should be considered.

References

Belytschko, T., Liu, W.K., Moran, B., 2000. Nonlinear Finite Elements for Continua and Structures. John Wiley & Sons, Ltd., Chichester.

Bridgman, P., 1949. The Physics of High Pressure. Bell and Sons, London.

Cockcroft, M.G., Latham, D.J., 1968. Ductility and the workability of metals. J. Inst. Met. 96, 33–39.

Dørum, C., Hopperstad, O.S., Lademo, O.-G., Langseth, M., 2003. Aluminium and magnesium castings—experimental work and numerical analyses. Int. J. Crashworthiness 8, 001–016.

Drucker, D.C., 1973. Plasticity theory, strength differential (SD) phenomenon, and volume expansion in metals and plastics. Metall. Trans. 4, 667.

Hydro Magnesium, 1998. Data Sheet, Die Cast Magnesium Alloys. Norsk Hydro.

Kelley, E.W., Hosford, H.F., 1968. The deformation characteristics of textured magnesium. Trans. Metall. Soc. AIME 242, 654–660.

Lademo, O.-G., 1999. Engineering Models of Elastoplasticity and Fracture for Aluminium Alloys, Dr. Ing. Thesis. Department of Structural Engineering, NTNU.

Laukli, H.I., 2002. Tensile Testing of AM60 U-profile. IMT, NTNU, Trondheim.

Li, M., Richmond, O., 1997. Intrinsic instability and nonuniformity of plastic deformation. Int. J. Plast. 13, 765–784.

LS-DYNA, 1998. Theoretical Manual. Livermore Software Technology Corporation, Livermore.

Rice, J.R., 1971. Inelastic constitutive relations for solids: an internal-variable theory and its application to metal plasticity. J. Mech. Phys. Solids 19, 443–455.

Sannes, S., Svalestuen, J.M., Dørum, C., Lademo, O.-G., 2003. Die Casting of Magnesium Alloys—Crash Requirements and Testing of Part Performance. Magnesium Automotive and End User Seminar, Aalen.

Simo, J.C., Taylor, R.L., 1985. Consistent tangent operators for rate-independent elastoplasticity. Comput. Meth. Appl. Mech. Eng. 48, 101–108.